

Determination of Critical Supersaturation from Microdroplet Evaporation Experiments

Guangwen He,^{†,‡} Venkateswarlu Bhamidi,^{†,#} Reginald B. H. Tan,^{‡,#} Paul J. A. Kenis,^{*,†} and Charles F. Zukoski^{*,†}

Department of Chemical & Biomolecular Engineering, University of Illinois at Urbana-Champaign, 600 South Mathews Avenue, Urbana, Illinois 61801, Department of Chemical & Biomolecular Engineering, National University of Singapore, 10 Kent Ridge Crescent, Singapore 119260, and Institute of Chemical & Engineering Sciences, 1 Pesek Road, Jurong Island, Singapore 627833

Received December 31, 2005; Revised Manuscript Received March 4, 2006

ABSTRACT: In this work, we identified a single critical supersaturation, the level of supersaturation above which nucleation will occur instantaneously, for each of a range of compounds: the amino acids glycine and L-histidine, the pharmaceutical paracetamol, the inorganic compound silicotungstic acid (STA), and the protein hen egg white lysozyme (HEWL). Using an evaporation-based microdroplet crystallization platform, we measured the time required to visually detect the first crystal. Crystals were observed to form at increasingly higher levels of supersaturation as the rate of evaporation was increased or as the initial solute concentration was reduced. Through extrapolation of all data of each compound to a nucleation time of zero, we identified a single point of high concentration, the critical supersaturation, which we found to be independent of the rate of solvent evaporation. Using the classical nucleation theory and thermodynamics, we correlated this critical supersaturation with surface tension between the nuclei and the surrounding media, and equilibrium solubility of the solute. This analysis suggests that, at conditions where supersaturation is generated very slowly, all compounds behave in a similar way such that the rate of nucleation at critical supersaturation is a constant fraction of the diffusion-limited rate of nucleation.

I. Introduction

Active pharmaceutical ingredients (APIs) are usually purified through crystallization processes in solution.¹ These molecules are “difficult” to crystallize due to their complex molecular structures, often requiring high levels of supersaturation and long induction times for crystals to be observed. These systems also typically crystallize into a variety of polymorphs. General techniques used to crystallize these molecules include temperature ramping, evaporation of solvent, and addition of anti-solvent. Control of crystallization in any of these processes is often limited by inadequate knowledge of crystal nucleation and growth kinetics. Many experimental and theoretical research efforts were geared toward increasing the understanding of crystallization kinetics.^{2–7}

As the rate of nucleation is often difficult to measure directly, alternative techniques are employed to obtain this kinetic information.⁸ Measurement of the induction time, the time one must wait to observe crystals after the solution has reached supersaturation, is the main approach used. The induction time is often considered to be inversely proportional to the nucleation rate and is extremely sensitive to the magnitude of supersaturation. Measurement of the metastable zone width (MZW) is another method used to acquire useful information about crystallization processes. MZW is the region between the solubility boundary (supersaturation = 1) and the metastable limit below which crystals do not form within a reasonable time period. For supersaturation levels above the metastable limit, crystals form rapidly. Several studies have estimated the width of the metastable zone experimentally, such that the rate at which the solution is quenched is instantaneous relative to the kinetics of the physical processes resulting in crystal formation.^{9–11} The

width of the metastable zone is found to depend on the method or path by which supersaturation is achieved, suggesting that rates of both heat and mass transfer are always important in determining the rate at which crystals form.

In this paper, we explore the effects of the rate of increasing supersaturation on the induction time and the MZW. In accordance with earlier studies,^{9–11} we found that the MZW increased with the rate of increase in supersaturation. However, we also found that if we started with increasingly larger initial concentrations of solute, the MZW became less dependent on the rate of increasing supersaturation, resulting in a critical value of supersaturation, where this dependence is lost and the induction time approaches zero. We refer to this supersaturation level as the critical supersaturation. We report that a broad class of materials including an API display similar dependence of the induction time on the rate of increase in supersaturation and initial solute concentration. We explain this dependence in terms of molecular properties through the solute solubility and the surface tension of the solid/liquid interface.

In section II, we describe the evaporation technique used in our studies to characterize the induction time as a function of initial solute concentration and rate of evaporation. In section III, we provide our results establishing the presence of a critical supersaturation and its dependence on material properties. Then in section IV, the classical nucleation theory is used to link the critical supersaturation to solubility and crystal surface tension. Finally, in section V we draw conclusions.

II. Experimental Section

Evaporation-Based Crystallization Platform. To rapidly generate kinetic data, we take advantage of an evaporation-based crystallization platform¹² that allows for the evaporation of solvent from a crystallizing droplet to the outside environment at a regulated rate through a channel of predefined geometry and dimensions (Figure 1). Gradual evaporation of the solvent drives the solution of the droplet to a condition conducive to a phase transition. A phase transition is ensured in every experiment since the final state of the droplet will always be a completely desiccated

* Corresponding authors: E-mail: (P.J.A.K.) kenis@uiuc.edu, (C.F.Z.) czukoski@uiuc.edu.

[†] University of Illinois at Urbana-Champaign.

[‡] National University of Singapore.

[#] Institute of Chemical & Engineering Sciences.

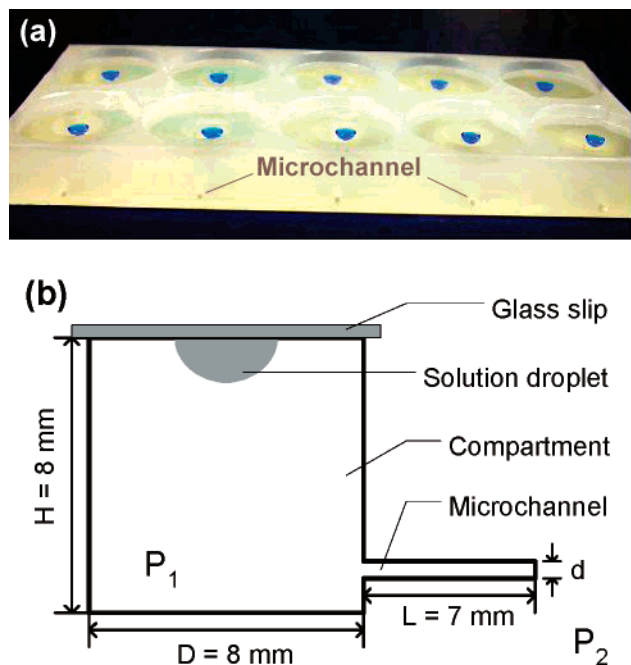


Figure 1. (a) A typical array of evaporation-based crystallization compartments in a polypropylene platform made by micro-machining; (b) Schematic diagram of an individual crystallization compartment. Typical dimensions for channel diameter d : 0.6 to 1.5 mm.

drop. Arrays of 10 of these crystallization compartments are micro-machined in a polypropylene block to allow for multiple experiments to be performed simultaneously (Figure 1).

The rate of droplet evaporation can be related to the channel geometry and ambient conditions through¹³

$$E = \frac{D}{RT} \left(P \ln \frac{P - P_2}{P - \gamma P_1} \right) \frac{A_c}{L} \quad (1)$$

where E is the flow rate of evaporating solvent out of the chamber, D is the diffusivity of solvent vapor in air, R is the gas constant, T is the absolute temperature, P is the total pressure while P_1 is the saturated vapor pressure of solvent, and P_2 is the partial pressure of solvent vapor in the laboratory environment. The activity coefficient of the solvent in the droplet is γ , while A_c and L are the cross-sectional area and length of the evaporation channel, respectively. Typical dimensions of the platforms used in this study are shown in Figure 1.

The abovementioned crystallization platform offers several advantages. First, each set of experiments takes less than a week and often less than 3 days; hence, many experiments can be performed in a short period of time. Second, the evaporation method allows for precise regulation of the rate of solvent evaporation by altering the dimensions of the evaporation channel, thus providing an opportunity to systematically study the effects of different rates of solvent evaporation (and thus the rate of increase in supersaturation) on nucleation. In addition, this method requires only minimal amounts of material because of the small sample volumes ($5 \mu\text{L}$) required for each experiment.

Solvent evaporation rates in our studies ranged from 29 to 446 $\mu\text{g}/\text{h}$. Prior to the experiments, we validated eq 1 by measuring the drying times of several solution droplets of known volume. These experimental drying times are in good agreement (within $\pm 5\%$) with the calculated drying times using eq 1. Thus, eq 1 describes the evaporation process adequately.

Experimental Methods. Glycine (Fluka, >99.5%), L-histidine (Fluka, >99.5%), and paracetamol (*N*-acetyl-4-aminophenol, Sigma, 98%) were dissolved in DI water (18 M Ω -cm, E-pure, Barnstead). Silicotungstic acid (STA, Sigma) was dissolved in DI water in the presence of LiCl. Hen egg white lysozyme (HEWL, Seikagaku, six times recrystallized) was dissolved in sodium acetate buffer (0.1 M, pH = 4.50) in the presence of NaCl. All chemicals were used without further purification. The solutions were filtered through 0.2 μm syringe filters (Nalgene) before being introduced to the crystallization platform.

Five-microliter droplets of solution were pipetted onto silanized glass slips (Hampton Research), and the glass slips were inverted and sealed on top of the evaporation compartment of the platform using high-vacuum grease (Dow Corning). The platforms were then left in a temperature- and humidity-controlled environment. To determine the nucleation time for each experiment, the droplets were checked for crystal formation regularly (time intervals range from 0.5 to 2 h) using an optical microscope (Leica MZ12.5). The limit of observation for this microscope is about 5 μm . Given known rapid crystal growth rates from literature,^{14–17} we can neglect the time between the actual nucleation of a crystal and the crystal reaching this minimum observable size (vide infra). After setting up the experiments, if no crystals were seen at, say, m hours, but crystals were apparent at n hours, then the nucleation time was taken as $(m + n)/2$. Typical numbers of crystals observed in our experiments range from 1 to 4. The experiments were carried out under different combinations of temperature and relative humidity (RH). Three replicates of each experiment were performed.

III. Results and Discussion

The crystallization behavior of several compounds in aqueous solution was explored. We started our studies by determining the nucleation time as a function of initial concentration of the solutes (glycine, L-histidine, paracetamol, STA, and HEWL) and the precipitating agents (LiCl and NaCl for STA and HEWL, respectively) at different evaporation rates (Figures 2 and 3). Note that the concentrations of solute and the precipitating agent (where present) increase with time as the evaporation progresses. For any given rate of evaporation within the range of our studies, we observed a linear relationship between the nucleation time and the initial solute concentration. Each line in Figures 2 and 3 represents a different evaporation rate of water. The experiments were highly reproducible with the resulting nucleation times being mostly within a standard deviation of about 10%.

Figure 2 shows experimental results of glycine crystallization. A line can be drawn through the induction times determined at a given rate of evaporation and extrapolated to an induction time of zero where the line intersects with the horizontal axis, suggesting that a solution will crystallize spontaneously without any water evaporation if prepared at that initial glycine concentration. If lines are drawn through induction times for different initial glycine concentration for each rate of evaporation, we observe that each extrapolated line intersects the horizontal axis at the same glycine concentration of $c_c \approx 225.5 \text{ g/L}$ ($T = 21 \text{ }^\circ\text{C}$, Figure 2b). At this temperature, the solubility of glycine c_s is 202 g/L,¹⁸ indicating that the critical supersaturation $S_c (= c_c/c_s)$ is 1.12. Similar results are obtained from crystallization experiments with the amino acid L-histidine, the pharmaceutical paracetamol, the inorganic compound STA, and the protein HEWL (Figure 3). For each of these compounds, all extrapolated lines intersect at a certain single concentration for an induction time of zero, leading to different values of S_c for each compound (Table 1).

The definition of critical supersaturation suggests that, if a solution is prepared with the solute concentration at its critical supersaturation, nucleation will occur in a very short period of time. We have verified this implication by crystallizing glycine, STA, and HEWL droplets at an initial solute concentration just at S_c . Nucleation occurred quickly in all three cases, and crystals could be seen within 20 min, a time period during which evaporation of solvent is insignificant. To further test this hypothesis, another set of crystallization experiments was conducted, in which droplets of glycine solution (184 g/L) were introduced into the platform under constant experimental conditions (21 $^\circ\text{C}$, 22% RH, and rate of evaporation = 131 $\mu\text{g}/\text{h}$). Then evaporation channels of the platform were sealed at different time points, giving different supersaturated states of

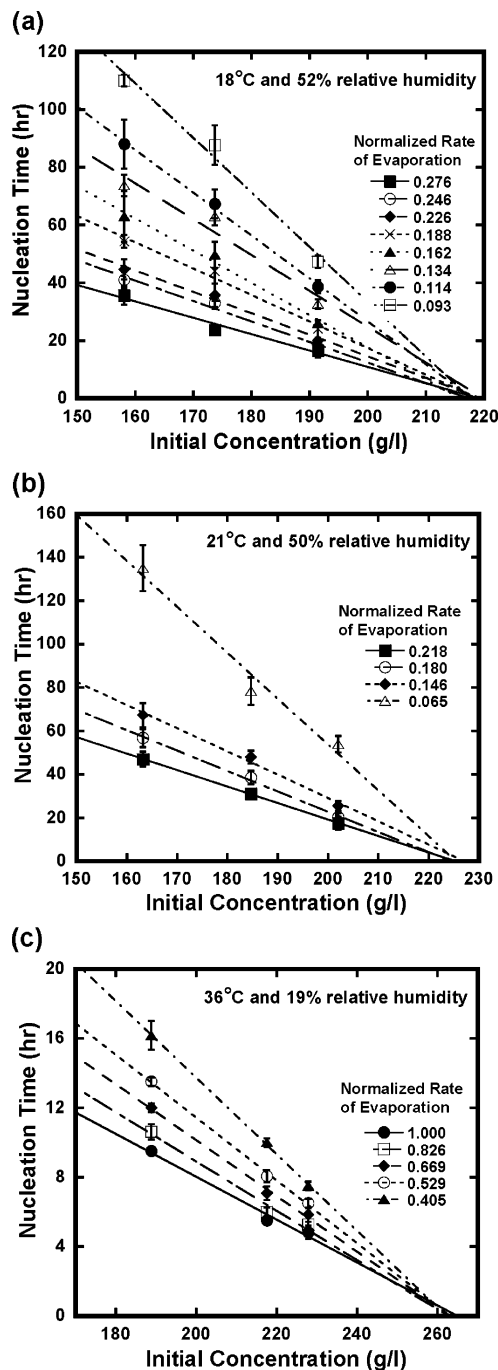


Figure 2. Nucleation time as a function of initial solute concentration of aqueous glycine solution for different evaporation rates at three different combinations of temperature and relative humidity (RH): (a) 18 °C and 52% RH; (b) 21 °C and 50% RH; and (c) 36 °C and 19% RH. In some cases, the error bars are smaller than the size of the data points. Normalized rate of evaporation 1.0 = 446 $\mu\text{g/h}$.

the solution droplets: (1) $1 < S < S_c$ ($S_c = 1.12$ in this case as determined previously); (2) $S = S_c$; and (3) $S > S_c$. For the droplets with supersaturation < 1.12 (experiment 1), no crystal formation was observed even after 24 h; however, for the droplets with supersaturation ≥ 1.12 (experiments 2 and 3), crystals formed in less than 2 h. These results indicate that S_c indeed represents a natural limiting point for nucleation in solutions that are slowly increased in concentration at a certain temperature.

Through a mass balance, the time-dependent concentration prior to crystal nucleation (i.e., for $t < t_n$, the nucleation time)

can be determined if the initial solute concentration c_0 and the rate of solvent evaporation E are known. From this information, we can determine the supersaturation in the solution droplet at t_n . We observe that fairly high supersaturations are reached when the initial concentration is low and the rate of evaporation is fast. Figure 4 shows that the supersaturation at different nucleation times $S(t_n)$ increases with an increasing rate of evaporation E and with a decreasing c_0 . These results are in accordance with numerous studies showing that the MZW increases with an increase in the rate of supersaturation.^{9–11} Our results specifically indicate that the width of the metastable zone also decreases as the initial solute concentration increases and becomes independent of rate of evaporation at S_c when t_n approaches zero.

IV. Origins of the Critical Supersaturation

To the best of our knowledge, this is the first report of a limiting point for the width of the metastable zone for nucleation of crystals from solution at certain temperature. We observe this phenomenon for a wide range of materials, from a large inorganic salt, to a protein, and to several organic molecules. This critical supersaturation is not a spinodal point, as evidenced by the following: First, when we quenched an aqueous glycine solution to a supersaturation level that is much higher than the critical supersaturation, no liquid–liquid separation was observed. Second, under the experimental conditions used (pH = 4.5 in 0.1 M NaAc buffer and 4.06% (w/v) NaCl), the critical supersaturation point determined at a lysozyme concentration of 34.7 mg/mL ($S \sim 10$) is well above the spinodal region reported in the literature.¹⁹

The value of the critical supersaturation S_c , which here varies over a range of 1–10 depending on the crystallizing compound, has a chemical specificity. When one measures an induction/nucleation time, one is actually measuring the sum of the time required to form a stable cluster and the time it takes for that cluster to grow into a crystal of observable size. From the literature, we know that the rates of crystal growth in our experiments are rapid;^{14–17} thus the time required for the crystal to grow to the observable size is insignificant in comparison with the time required to nucleate a stable cluster. We are interested in understanding how the rate of nucleation at S_c varies for different solutes and initiate our analysis with the classical nucleation theory, which relates the nucleation rate J to the supersaturation and surface tension σ :^{3,4,20}

$$J = AS \exp\left(\frac{-B}{\ln^2 S}\right) \quad (2)$$

where the preexponential factor A , sometimes referred to as the diffusion-limited rate of nucleation, is practically independent of the supersaturation S that is defined as

$$S = \frac{\gamma c}{\gamma_e c_e} \quad (3)$$

In eq 3, γ and γ_e are the activity coefficients of the solvent molecules in the solution with solute concentration c and c_e (solubility), respectively. The preexponential factor A can be interpreted as the diffusion-limited rate of nucleation and is a complicated function of molecular properties.^{3,4,20} The thermodynamic parameter B is given by^{3,4,20}

$$B = \frac{16\pi v^2 \sigma^3}{3(kT)^3} \quad (4)$$

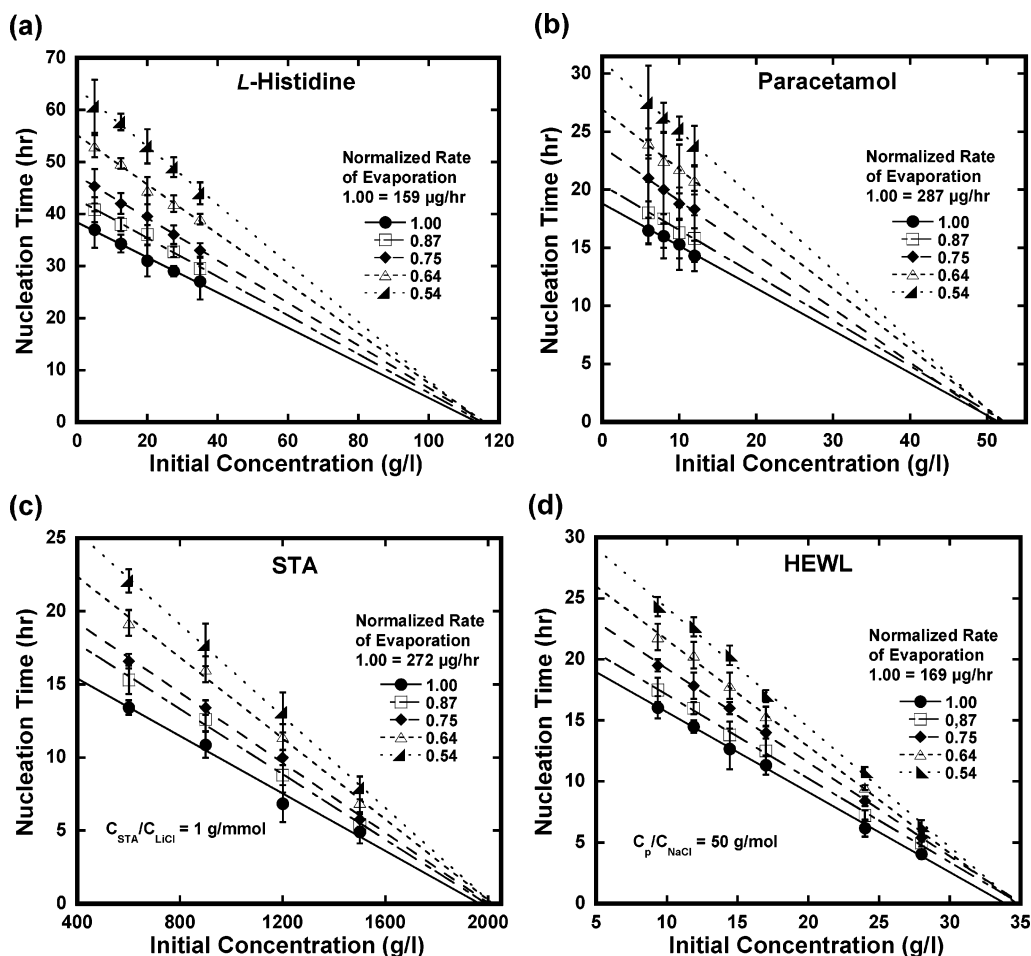


Figure 3. Nucleation time vs initial solute concentration of four compounds for different rates of evaporation under different combinations of temperature and RH: (a) L-histidine, 18 °C and 50% RH; (b) paracetamol, 21 °C and 16% RH; (c) silicotungstic acid (STA), 21 °C and 18% RH. The LiCl concentrations range from 0.6 to 1.5M; and (d) hen egg white lysozyme (HEWL), 21 °C and 24% RH. The NaCl concentrations range from 1.09 to 3.28% (w/v). The ratios of the solute and salt concentrations, which stay inherently constant throughout each experiment, are specified in panels c and d.

Table 1. Average Extrapolated Critical Concentration and Critical Supersaturation for Different Compounds Crystallizing under Various Conditions^a

compound	solubility c_e (g/L)	extrapolated critical conc c_c (g/L)	critical supersaturation $S_c = \gamma_c c_c / \gamma_e c_e \approx c_c / c_e$
glycine (36°C)	256.2	263.8	1.03
glycine (21°C)	202.0	226.2	1.12
glycine (18°C)	191.4	218.2	1.14
STA (21°C)	1056.0	1995.8	1.89
L-histidine (18°C)	36.2	115.1	3.18
paracetamol (21°C)	13.2	50.8	3.85
HEWL (21°C)	3.4	34.7	10.22

^a Glycine (in water), STA (2 M LiCl, water), L-histidine (water), paracetamol (water), and HEWL (4.06% (w/v) NaCl, 0.1M acetate buffer, pH = 4.50). Activity coefficients for water in solutions with critical and saturated concentrations of solute, γ_c and γ_e , respectively, are approximately equal.

where v is the molecular volume ($= \pi d^3/6$ for a spherical nucleus with diameter d), σ is the surface tension, k is the Boltzmann constant, and T is the absolute temperature. When the solute concentration is set at its critical value S_c , a critical rate of nucleation J_c can be defined. Thus, rearranging eq 2 in terms of S_c yields:

$$\ln^3 S_c + \ln(A/J_c) \ln^2 S_c - B = 0 \quad (5)$$

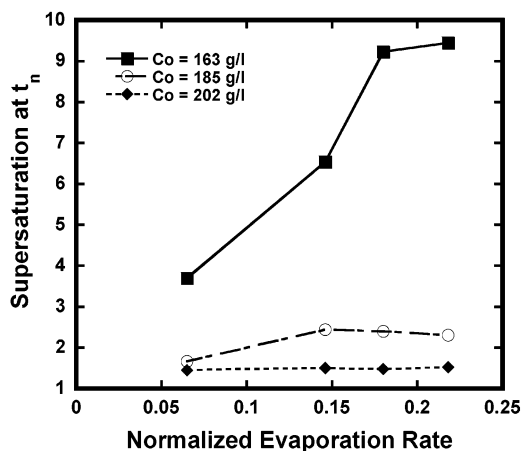


Figure 4. Supersaturation at nucleation time $S(t_n)$ as a function of evaporation rate for different initial glycine concentrations ($T = 21$ °C, RH = 50%). Normalized rate of evaporation 1.0 = 446 $\mu\text{g/h}$.

The fraction of the limiting rate of nucleation (J_c/A) that occurs at S_c can be estimated using eq 5 as long as the parameter B can be evaluated. This requires knowledge of the surface tension between the nuclei and the surrounding media, for which purpose one can exploit correlations between surface tension and solubility. The surface tension σ between the nuclei and

Table 2. Calculated Values of Surface Tensions σ and Thermodynamic Parameters B from Solubility c_e , Solid Density n_{cr} , Molecular Size d , and Equilibrium Activity Coefficient γ_e Using Christoffersen's Correlation²⁴

compound	solubility c_e (g/L)	solid density n_{cr} (g/L)	molecular size d (nm)	activity coefficient γ_e	surface tension σ (mJ/m ²)	B
glycine (36°C)	256.2	1160	0.53	0.91	7.75	0.61
glycine (21°C)	202.0	1160	0.53	0.93	8.37	0.89
glycine (18°C)	191.4	1160	0.53	0.93	8.53	0.98
STA (21°C)	1056.0	6620	1.20	0.40	2.47	3.09
L-histidine (18°C)	36.2	1440	0.70	0.97	9.79	7.59
paracetamol (21°C)	13.2	1290	0.72	0.98	11.63	14.44
HEWL (21°C)	3.4	1240	3.40	0.58	0.72	39.64

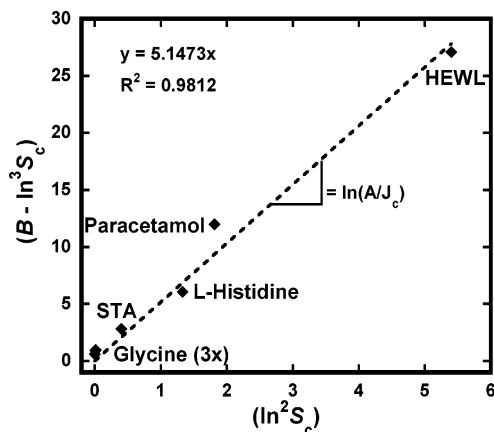
the surrounding mother solution is strongly correlated to their solubility c_e .^{21–24} Nielsen and Söhnel²¹ introduced a common linear relationship between σ and $\ln(c_e)$ for 32 electrolytes in aqueous solution. Bennema and Söhnel,²² and Mersmann²³ independently extended this analysis on electrolytes by applying regular solution theory and classical thermodynamics, respectively. Moreover, Christoffersen et al.²⁴ re-derived the relation based on surface nucleation using fewer assumptions than the previous studies.^{21–23}

Following the analysis of Christoffersen et al.,²⁴ we link solubility and crystal surface tension as

$$\frac{\sigma d^2}{kT} = \frac{1}{\pi} \ln\left(\frac{n_{cr}}{\gamma_e c_e}\right) \quad (6)$$

where $\sigma d^2/kT$ is the dimensionless surface tension and n_{cr} is the density of crystal. Values for the density of crystals n_{cr} of the respective materials are obtained either from the Material Safety Data Sheet (MSDS) for glycine, L-histidine, and paracetamol, or from the literature for STA and HEWL.^{25,26} Values for the solubility of each of the compounds c_e are obtained from various literature sources.^{18,25,27–29} Values for the respective molecular sizes d are either estimated from unit cell parameters for glycine, L-histidine, and paracetamol,^{30–32} or obtained from the literature for STA and HEWL.^{25,33} Values for the respective activity coefficients γ_e are obtained from the literature for glycine,³⁴ and are estimated from an approach introduced by Lewis and Randall³⁵ for the other compounds. Table 2 lists the calculated surface tensions and values of B for all five compounds used in this study.

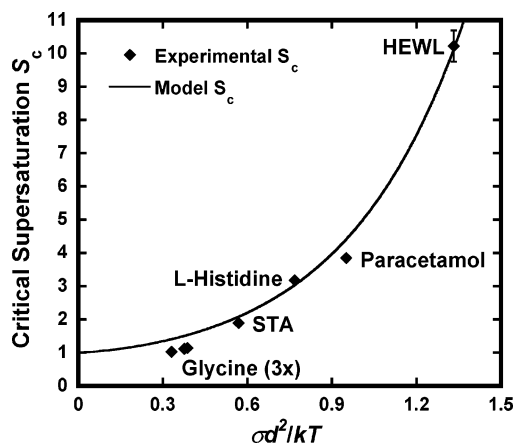
With the value of B estimated, we rearrange eq 5 to determine a value of 5.15 for $\ln(A/J_c)$ from the slope of a plot of $(B - \ln^3 S_c)$ as a function of $(\ln^2 S_c)$ as shown in Figure 5. That the nucleation rate at the critical supersaturation is the same fraction of the diffusion-limited rate of nucleation A ($J_c/A = 0.0058$) for all the compounds investigated is surprising. Figure 6 shows the

**Figure 5.** Plot of $(B - \ln^3 S_c)$ versus $(\ln^2 S_c)$ for different compounds. From eq 5, it follows that the slope of this plot equals $\ln(A/J_c)$.

critical supersaturation as a function of solid/liquid surface tension and reveals a remarkable agreement between experiment and the model (eq 5, with $\ln(A/J_c) = 5.15$). Note that in this case the surface tension is calculated from physical properties that are totally independent from nucleation data, suggesting that from knowledge of solubility and crystal density, one can estimate the surface tension, and from this value, the critical supersaturation. Several studies have shown that the classical nucleation theory captures the energy barrier for nucleation well but has difficulties predicting the absolute magnitude of the nucleation rate, often being off by many orders of magnitude.^{3,4,20} That the critical supersaturation as determined in the experiments carried out here occurs at some fixed fraction of the fastest possible rate of nucleation is truly intriguing.

Several features of the data are worthy of comment. First, the data in Figure 6 indicate that as the solubility of the material in question decreases, the critical supersaturation increases. Indeed, those materials with the highest solubilities have the lowest surface tensions and thus the lowest values of S_c . Second, the correlation developed here is demonstrated for a variety of compounds that crystallize into a variety of point groups with a variety of crystal packing. Thus, we anticipate that the existence of the critical supersaturation is a general phenomenon for small and large molecules, suggesting that nucleation occurs in similar ways for each of them. Finally, when in the limit of low surface tensions, S_c approaches unity.

In sum, the critical supersaturation described here is determined by increasing the solute concentration extremely slowly. Under these conditions, our theoretical analysis presented here based on the classical nucleation theory suggests that all compounds behave in a similar way such that the rate of

**Figure 6.** Comparison of experimental data and model predictions for critical supersaturation as a function of dimensionless surface tension, $\sigma d^2/kT$. Experimental conditions are glycine (18, 21, and 36 °C, in water), STA (21 °C, LiCl, water), L-histidine (18 °C, water), paracetamol (21 °C, water), and HEWL (21 °C, NaCl, 0.1M acetate buffer, pH = 4.50). The calculated curve is obtained by setting $\ln(A/J_c) = 5.15$. In most cases, the error bars are smaller than the size of the data points.

nucleation at this point is a constant fraction of the diffusion-limited rate of nucleation.

V. Conclusion

In this paper, we have systematically studied the crystallization of several chemical compounds (glycine, L-histidine, paracetamol, STA, and HEWL) using an evaporation-based crystallization platform that enables precise control over solvent evaporation.¹² We observed a linear relationship between nucleation time and initial solute concentration at different rates of evaporation. Also, we have identified a certain supersaturation above which spontaneous nucleation occurs instantaneously, the *critical supersaturation*, for each of these compounds.

We have correlated this critical supersaturation to solubility of the solute and surface tension between the nuclei and the surrounding media through well-established concepts of the classical nucleation theory and thermodynamics. The calculated values of critical supersaturation and the experimental results are in good agreement. This correlation gives rise to the possibility of an a priori prediction of the experimentally difficult-to-access critical supersaturation for many compounds from a readily available physical property, the solubility. This result may find direct application in industrial crystallization as the critical supersaturation provides a boundary as an operational guideline for crystallization. In addition, the correlation among solubility, surface tension, and critical supersaturation may provide a plausible explanation of polymorph selectivity in solution crystallization.

We are currently developing a dynamic model to simulate the crystallization process by solvent evaporation. This model would offer more physical insight about the kinetics of crystallization and the phenomenon of critical supersaturation.

Acknowledgment. The authors thank Professor Richard D. Braatz and Michael Mitchell from the University of Illinois at Urbana-Champaign for stimulating discussions. Sincere gratitude is also expressed to the Agency for Science, Technology and Research (A*STAR), Singapore, and the National Institute of Health (NIH), USA (Grant No. 1 R21 GM075930-01) for their generous financial support, without which this research would have been impossible.

References

- (1) Rodríguez-Hornedo, N.; Murphy, D. *J. Pharm. Sci.* **1999**, *88*, 651–660.
- (2) Nielsen, A. E. *Kinetics of Precipitation*; Pergamon Press: Glasgow, 1964.
- (3) Zettlemoyer, A. C., Ed. *Nucleation*; Marcel Dekker: New York, 1969.
- (4) Kashchiev, D. *Nucleation: Basic Theory with Applications*; Butterworth-Heinemann: Oxford, 2000.
- (5) Vekilov, P. G. *Cryst. Growth Des.* **2004**, *4*, 671–685.
- (6) Kulkarni, A. M.; Zukoski, C. F. *Langmuir* **2002**, *18*, 3090–3099.
- (7) Bhamidi, V.; Varanasi, S.; Schall, C. A. *Langmuir* **2005**, *21*, 9044–9050.
- (8) Garside, J.; Mersmann, A.; Nývlt, J., Eds. *Measurement of Crystal Growth and Nucleation Rates*; Institution of Chemical Engineers: Rugby, 2002.
- (9) Nývlt, J. *J. Cryst. Growth* **1968**, *3–4*, 377–383.
- (10) Kim, K.-J.; Mersmann, A. *Chem. Eng. Sci.* **2001**, *56*, 2315–2324.
- (11) Mersmann, A.; Bartosch, K. *J. Cryst. Growth* **1998**, *183*, 240–250.
- (12) Talreja, S.; Kim, D. Y.; Mirarefi, A. Y.; Zukoski, C. F.; Kenis, P. J. *A. J. Appl. Crystallogr.* **2005**, *38*, 988–995.
- (13) Geankoplis, C. J. *Transport Processes and Unit Operations*, 3rd ed.; Prentice Hall P T R: Englewood Cliffs, 1993.
- (14) Li, L.; Rodríguez-Hornedo, N. *J. Cryst. Growth* **1992**, *121*, 33–38.
- (15) Finnie, S. D.; Ristic, R. I.; Sherwood, J. N.; Zikic, A. M. *J. Cryst. Growth* **1999**, *207*, 308–318.
- (16) Saikumar, M. V.; Glatz, C. E.; Larson, M. A. *J. Cryst. Growth* **1998**, *187*, 277–288.
- (17) Forsythe, E.; Pusey, M. L. *J. Cryst. Growth* **1994**, *139*, 89–94.
- (18) Fasman, G. D., Ed. *Handbook of Biochemistry and Molecular Biology*, Physical and Chemical Data; CRC Press: Cleveland, 1975; Vol. I.
- (19) Muschol, M.; Rosenberger, F. *J. Chem. Phys.* **1997**, *107*, 1953–1962.
- (20) Debenedetti, P. G. *Metastable Liquids: Concepts and Principles*; Princeton University Press: Princeton, 1995.
- (21) Nielsen, A. E.; Söhnel, O. *J. Cryst. Growth* **1971**, *11*, 233–242.
- (22) Bennema, P.; Söhnel, O. *J. Cryst. Growth* **1990**, *102*, 547–556.
- (23) Mersmann, A. *J. Cryst. Growth* **1990**, *102*, 841–847.
- (24) Christoffersen, J.; Rostrup, E.; Christoffersen, M. R. *J. Cryst. Growth* **1991**, *113*, 599–605.
- (25) Ramakrishnan, S.; Zukoski, C. F. *J. Chem. Phys.* **2000**, *113*, 1237–1248.
- (26) Leung, A. K. W.; Park, M. M. V.; Borhani, D. W. *J. Appl. Crystallogr.* **1999**, *32*, 1006–1009.
- (27) Ajinomoto Co., Inc. http://www.ajinomoto.co.jp/amino/e_aminoscience/bc/amino_08.html.
- (28) Granberg, R. A.; Rasmuson, A. C. *J. Chem. Eng. Data* **1999**, *44*, 1391–1394.
- (29) Forsythe, E. L.; Judge, R. A.; Pusey, M. L. *J. Chem. Eng. Data* **1999**, *44*, 637–640.
- (30) Marsh, R. E. *Acta Crystallogr.* **1958**, *11*, 654–663.
- (31) Madden, J. J.; McGandy, E. L.; Seeman, N. C. *Acta Crystallogr. B* **1972**, *28*, 2377–2382.
- (32) Nichols, G.; Frampton, C. S. *J. Pharm. Sci.* **1998**, *87*, 684–693.
- (33) Mikol, V.; Hirsch, E.; Giege, R. *J. Mol. Biol.* **1990**, *213*, 187–195.
- (34) Na, H.-S.; Arnold, S.; Myerson, A. S. *J. Cryst. Growth* **1994**, *139*, 104–112.
- (35) Snoeyink, V. L.; Jenkins, D. *Water Chemistry*; John Wiley & Sons: New York, 1980.

CG050681F